

## Electron effective mass and mobility limits in degenerate perovskite stannate BaSnO<sub>3</sub>

Christian A. Niedermeier,<sup>1,2,3,\*</sup> Sneha Rhode,<sup>1</sup> Keisuke Ide,<sup>2</sup> Hidenori Hiramatsu,<sup>2,3</sup> Hideo Hosono,<sup>2,3</sup> Toshio Kamiya,<sup>2,3</sup> and Michelle A. Moram<sup>1</sup>

<sup>1</sup>*Department of Materials, Imperial College London, Exhibition Road, London SW7 2AZ, United Kingdom*

<sup>2</sup>*Laboratory for Materials and Structures, Tokyo Institute of Technology, Mailbox R3-4, 4259 Nagatsuta, Midori-ku, Yokohama 226-8503, Japan*

<sup>3</sup>*Materials Research Center for Element Strategy, Tokyo Institute of Technology, 4259 Nagatsuta, Midori-ku, Yokohama 226-8503, Japan*  
(Received 18 September 2016; revised manuscript received 15 February 2017; published 11 April 2017)

The high room temperature mobility and the electron effective mass in BaSnO<sub>3</sub> are investigated in depth by evaluation of the free carrier absorption observed in infrared spectra for epitaxial films with free electron concentrations from  $8.3 \times 10^{18}$  to  $7.6 \times 10^{20}$  cm<sup>-3</sup>. Both the optical band gap widening by conduction band filling and the carrier scattering mechanisms in the low- and high-doping regimes are consistently described employing parameters solely based on the intrinsic physical properties of BaSnO<sub>3</sub>. The results explain the current mobility limits in epitaxial films and demonstrate the potential of BaSnO<sub>3</sub> to outperform established wide-band gap semiconductors also in the moderate doping regime.

DOI: [10.1103/PhysRevB.95.161202](https://doi.org/10.1103/PhysRevB.95.161202)

Transparent perovskite stannate BaSnO<sub>3</sub> shows great potential as a high-mobility electron transport material composed of abundant elements. Since the report of an extraordinary high room temperature mobility of 320 cm<sup>2</sup>/V s for La:BaSnO<sub>3</sub> single crystals [1], which is the highest value reported for perovskite oxides, the material has rapidly attracted interest as a high-mobility channel layer in oxide thin film transistors [2–4] and multifunctional perovskite-based optoelectronic devices [5,6]. To fully exploit the potential of La:BaSnO<sub>3</sub> for device applications, current research concentrates on understanding and improving the electron transport in epitaxial La:BaSnO<sub>3</sub> thin films [7–14].

La:BaSnO<sub>3</sub> thin films grown heteroepitaxially on SrTiO<sub>3</sub> substrates using pulsed laser deposition (PLD) show a reduced carrier mobility of 70 cm<sup>2</sup>/V s [7] as compared to single crystals. It was suggested that the high density of dislocations introduced scattering centers for electron transport [8]. However, even by homoepitaxy on BaSnO<sub>3</sub> single crystals the carrier mobility can be increased only to 100 cm<sup>2</sup>/V s [13]. Moreover, molecular beam epitaxy allows for preparation of La:BaSnO<sub>3</sub> films with the record Hall mobility of 124 cm<sup>2</sup>/V s on SrTiO<sub>3</sub> substrates [12], suggesting the larger impact of the deposition method on electron transport properties. A quantitative analysis of the prevailing carrier scattering mechanism in BaSnO<sub>3</sub> is still lacking and would provide a guideline for improving the electron transport beyond the current mobility limits of epitaxial films.

The high mobility in La:BaSnO<sub>3</sub> single crystals is attributed to the large dispersion of the Sn 5s orbital-derived conduction band and the ideal 180° O-Sn-O bond angle in the network of corner-sharing (SnO<sub>6</sub>)<sup>2-</sup> octahedra in the cubic perovskite structure [15]. Quantitatively, the electron mobility is given by

$$\mu = \frac{e\tau}{m_e^*}, \quad (1)$$

where  $e$  is the electron charge,  $m_e^*$  is the electron effective mass, and  $\tau$  is the relaxation time denoting the average time of

momentum loss by scattering. A fundamental understanding of the electron transport in epitaxial La:BaSnO<sub>3</sub> films thus requires a quantitative analysis of the effective mass  $m_e^*$  and scattering relaxation time  $\tau$ , which are both strongly dependent on carrier concentration.

This work presents an in-depth quantitative analysis of the La:BaSnO<sub>3</sub> electron effective mass by evaluation of the free carrier absorption observed in infrared spectra for a wide range of carrier concentrations from  $8.3 \times 10^{18}$  to  $7.6 \times 10^{20}$  cm<sup>-3</sup>. The nonparabolicity of the La:BaSnO<sub>3</sub> conduction band is derived from the dependence of electron effective mass on doping level. The results are employed in an analytical model to consistently describe the optical band gap widening due to conduction band filling, by taking the band gap narrowing induced by electron-electron and electron-impurity interactions into account. The current mobility limits in La:BaSnO<sub>3</sub> epitaxial films are described well by the analytical models for electron scattering by longitudinal optical (LO) phonons, dislocations, and ionized impurities for degenerate doping.

200-nm epitaxial La:BaSnO<sub>3</sub> thin films were grown by PLD on 50-nm NiO-buffered MgO substrates to reduce the lattice mismatch to less than 1.4%. The experimental details for thin film growth are provided in the Supplemental Material [16]. The 204 reciprocal space map high-resolution X-ray diffraction (HR-XRD) analysis confirms the [100] epitaxial orientation of the La:BaSnO<sub>3</sub> thin film on NiO-buffered MgO substrate [Fig. 1(a)]. The NiO buffer layer is slightly strained in plane while the La:BaSnO<sub>3</sub> thin film is completely relaxed and shows a moderate degree of mosaicity as indicated by the broadened diffraction peak relative to that of the MgO single crystal.

The cross-sectional bright field transmission electron microscopy (TEM) image of the La:BaSnO<sub>3</sub> thin film on a NiO-buffered MgO substrate indicates columnar growth as deduced from the observation of grain boundaries marked by the arrows in Fig. 1(b). The cross-sectional high-resolution micrograph shows that the La:BaSnO<sub>3</sub>/NiO interface is free of misfit dislocations [Fig. 1(c)] as confirmed by the average background subtraction-filtered (ABSF) HR-TEM micrograph

\*Corresponding author: [c.niedermeier13@imperial.ac.uk](mailto:c.niedermeier13@imperial.ac.uk)

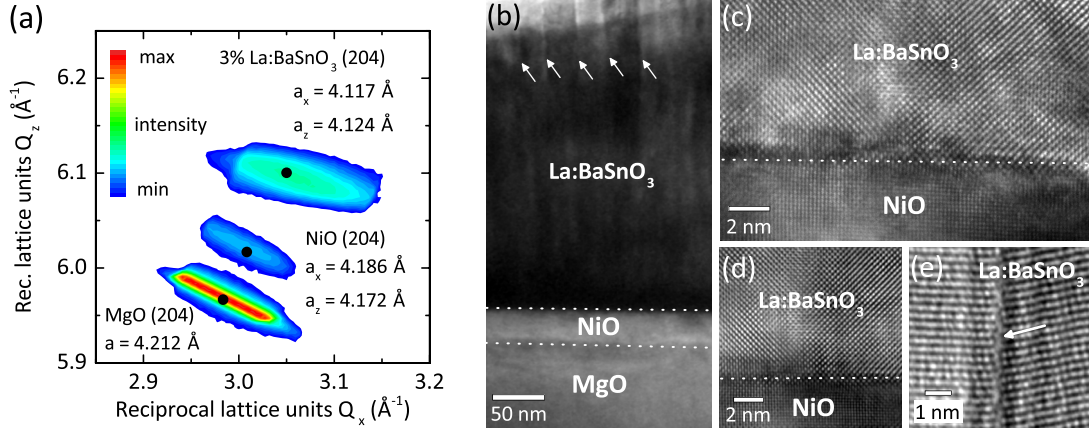


FIG. 1. (a) HR-XRD 204 reciprocal space map of La:BaSnO<sub>3</sub> thin film on NiO-buffered MgO substrate given by an intensity contour map on a logarithmic scale with reference positions of unstrained crystals indicated by black dots. (b) Cross-sectional bright field TEM micrograph indicates the presence of vertical grain boundaries in La:BaSnO<sub>3</sub> and columnar growth. (c) Cross-sectional HR-TEM micrograph shows the single-domain epitaxy at the La:BaSnO<sub>3</sub>/NiO interface which is free of misfit dislocations as confirmed by the (d) ABSF-filtered HR-TEM micrograph. (e) HR-TEM micrograph of a low-angle grain boundary between two La:BaSnO<sub>3</sub> crystallites.

[Fig. 1(d)]. Consistent with the mosaicity derived from HR-XRD analysis, the La:BaSnO<sub>3</sub> microstructure shows grains of about 30 nm size which are slightly tilted with respect to the [100] epitaxial orientation and forms low-angle grain boundaries [Fig. 1(e)].

Optical transmittance and reflectivity spectra of La:BaSnO<sub>3</sub> films were measured by vacuum Fourier transform infrared (FTIR) spectroscopy for photon energies of 0.1 to 1 eV. Furthermore, reflection spectroscopic ellipsometry was used to investigate the La:BaSnO<sub>3</sub> dielectric function in the spectral range from 0.6 to 4.8 eV. The optical dielectric function  $\epsilon(\omega)$  of La:BaSnO<sub>3</sub> is extracted by simultaneously fitting a combined model of the Drude free carrier absorption and the Tauc-Lorentz dispersion function to the ellipsometry and FTIR spectra [16]. The IR dielectric function is described by the Drude free electron model

$$\epsilon(\omega) = \epsilon_{\infty} - \frac{\epsilon_{\infty} \omega_p^2}{\omega^2 - i\gamma_p \omega}, \quad (2)$$

where  $\epsilon_{\infty}$  is the optical dielectric constant,  $\omega_p$  is the plasma frequency,  $\omega$  is the photon frequency, and  $\gamma_p$  is the broadening frequency. The parameters used in the analytical model allow for calculation of the electron effective mass

$$m_e^* = \frac{ne^2}{\epsilon_0 \epsilon_{\infty} \omega_p^2}, \quad (3)$$

where  $\epsilon_0$  is the vacuum dielectric constant and  $n$  is the carrier concentration, determined from alternating current Hall measurements. The La:BaSnO<sub>3</sub> electron effective mass increases remarkably from 0.19 to 0.36 $m_0$  for carrier concentrations from  $1.6 \times 10^{19}$  to  $7.6 \times 10^{20}$  cm<sup>-3</sup>, respectively (Fig. 2).

The energy dispersion  $E$  of electrons near the conduction band minimum can be described by a first-order nonparabolicity approximation [18]

$$\frac{\hbar^2 k^2}{2m_{e0}^*} = E(1 + \beta E), \quad (4)$$

where  $\hbar$  is the reduced Planck constant,  $m_{e0}^*$  is the electron effective mass at the conduction band minimum,  $k = (3n\pi^2)^{1/3}$  is the Fermi wave vector, and  $\beta$  is an empirical fitting parameter describing the degree of nonparabolicity of the conduction band. After solving the quadratic equation (4) to obtain the electron energy  $E$  and applying the relation [19]

$$\frac{1}{m_e^*} = \frac{1}{\hbar^2 k} \frac{dE}{dk}, \quad (5)$$

the effective mass is given by

$$m_e^* = m_{e0}^* \sqrt{1 + 2\beta \frac{\hbar^2 k^2}{m_{e0}^*}}. \quad (6)$$

Fitting of Eq. (6) to the electron effective mass data yields  $m_{e0}^* = 0.19 \pm 0.02 m_0$  at the conduction band minimum,

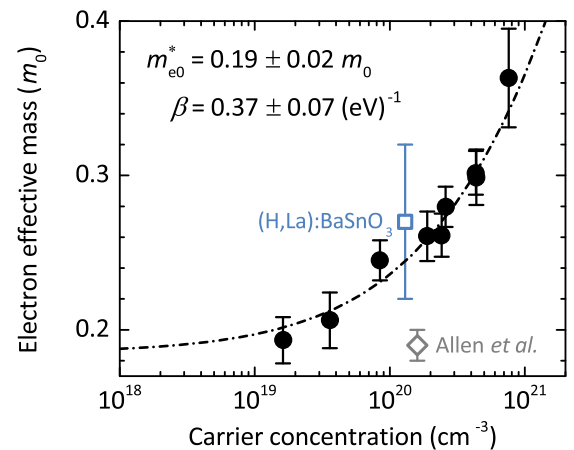


FIG. 2. Increase in La:BaSnO<sub>3</sub> electron effective mass with carrier concentration as determined by the plasma frequency in the Drude model for free carrier absorption (black filled circles). The IR dielectric function was obtained from transmittance/reflectivity FTIR and ellipsometry spectra. The effective mass of co-doped (H,L)La:BaSnO<sub>3</sub> determined in a previous analysis [14] and that of La:BaSnO<sub>3</sub> determined by Allen *et al.* [17] are given for comparison.

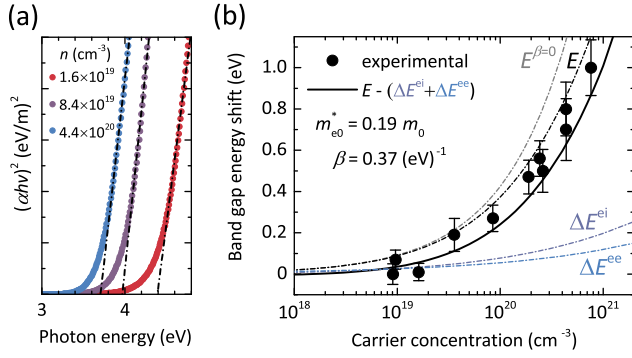


FIG. 3. (a) Optical absorption spectra plotted for a direct-type transition. The optical band gap shifts from 3.7 to 4.4 eV when the carrier concentration increases from  $1.6 \times 10^{19}$  to  $4.4 \times 10^{20} \text{ cm}^{-3}$ . (b) Increase in the La:BaSnO<sub>3</sub> optical band gap with carrier concentration due to conduction band filling effect, where  $E^{\beta=0}$  is the energy of electrons assuming a parabolic band dispersion. The theoretical model employs the effective mass and nonparabolicity parameter derived from the optical analysis to calculate the energy dispersion  $E$  of conduction band electrons. The band gap narrowing due to electron-impurity ( $\Delta E_g^{\text{ei}}$ ) and electron-electron interactions ( $\Delta E_g^{\text{ee}}$ ) is taken into account.

in good agreement with the result from hybrid density functional theory [20]. The nonparabolicity parameter  $\beta = 0.37 \pm 0.07 \text{ (eV)}^{-1}$  indicates a more pronounced increase in the La:BaSnO<sub>3</sub> effective mass with carrier concentration as compared to other transparent conducting oxides such as Ga:ZnO [ $\beta = 0.14 \text{ (eV)}^{-1}$ ] and Sn:In<sub>2</sub>O<sub>3</sub> [ $\beta = 0.18 \text{ (eV)}^{-1}$ ] [21], and a significant dependence of mobility on doping level.

The ellipsometry spectra in the energy range from 0.6 to 4.8 eV were analyzed to extract the La:BaSnO<sub>3</sub> optical band gap independently from that of the NiO buffer layer and investigate the Burstein-Moss shift [16]. The optical band gap was determined from a plot of  $(\alpha h\nu)^2$  vs photon energy  $h\nu$ , where  $\alpha$  denotes the absorption coefficient, which is valid for a direct transition at the absorption edge [Fig. 3(a)]. Due to the conduction band filling effect, the La:BaSnO<sub>3</sub> optical absorption edge shifts from 3.7 to 4.4 eV when the carrier concentration increases from  $1.6 \times 10^{19}$  to  $4.4 \times 10^{20} \text{ cm}^{-3}$ .

With increasing carrier concentration, electron-electron and electron-impurity interactions partially compensate the Burstein-Moss shift as the conduction band edge is shifted to lower energies. The band gap narrowing due to the electron-electron interactions is given by [22]

$$\Delta E_g^{\text{ee}} = \frac{e^2 k}{2\pi^2 \epsilon_s \epsilon_0} + \frac{e^2 \lambda}{8\pi \epsilon_s \epsilon_0} \left[ 1 - \frac{4}{\pi} \tan^{-1} \left( \frac{k}{\lambda} \right) \right], \quad (7)$$

where  $\epsilon_s = 21$  [23,24] is the BaSnO<sub>3</sub> static dielectric constant,  $\lambda = 2\sqrt{k/a_B^* \pi}$  is the Thomas-Fermi screening length,  $a_B^* = 4\pi \epsilon_s \epsilon_0 \hbar^2 / m_e^* e^2$  is the effective Bohr radius, and  $\hbar$  is the reduced Planck constant. The band gap narrowing due to the electron-impurity interactions is given by

$$\Delta E_g^{\text{ei}} = \frac{ne^2}{\epsilon_s \epsilon_0 a_B^* \lambda^3}. \quad (8)$$

In total, both effects contribute to approximately 0.2 eV narrowing of the optical band gap for the highest electron concentration of  $7.6 \times 10^{20} \text{ cm}^{-3}$ . After subtraction of the conduction band shifts, the Burstein-Moss shift in La:BaSnO<sub>3</sub> is described consistently with Eq. (4), employing the effective mass and the nonparabolicity parameter obtained from optical spectra analysis [the solid curve in Fig. 3(b)]. As compared to a previous analysis of the Burstein-Moss shift of the indirect electronic band gap of La:BaSnO<sub>3</sub> determined by photoelectron spectroscopy [25], the present results indicate a more pronounced nonparabolicity of the conduction band and a weaker effect of many-body electron-electron and electron-impurity interactions.

After determination of the effective mass, the mobility in La:BaSnO<sub>3</sub> can be quantitatively described using Eq. (1) and adopting an analytical description of the relaxation time for carrier scattering. The temperature-dependent electron transport properties for 0.3, 1.5, and 5 at.% La-doped films show degenerate, metal-like behaviors characterized by a constant carrier concentration [16] and only moderately increasing Hall mobility with decreasing temperature from 300 to 45 K [Fig. 4(a)]. Since the La (0/+ charge transition level in BaSnO<sub>3</sub> lies within the conduction band [20], it may be assumed that all the La atoms are readily ionized to donate an electron to the reservoir of free carriers. However, for small doping levels the Hall carrier concentration is significantly reduced as compared to the La impurity concentration [16]. The La:BaSnO<sub>3</sub> films of less than 0.3 at.% La impurity concentration ( $n_{\text{La}} = 4 \times 10^{19} \text{ cm}^{-3}$ ) are highly resistive, which suggests trapping of free carriers by defects in the microstructure. Above a doping level of 0.3 at.% La, the room-temperature Hall mobility increases from 18 to 70 cm<sup>2</sup>/V s at carrier concentrations from  $8.3 \times 10^{18}$  to  $4.4 \times 10^{20} \text{ cm}^{-3}$ , respectively, but then drops at higher carrier concentrations [Fig. 4(b)].

The crystal mosaicity observed in the HR-XRD analysis and the microstructure in the TEM observation suggest the vertical grain boundaries as possible carrier traps. However, the activation energy of mobility, which reflects the electron transport potential barrier height and temperature-dependent scattering properties, are as low as 2.5–3.6 meV and significantly smaller than the thermal energy  $k_B T$ , where  $k_B$  is the Boltzmann constant and  $T$  is the absolute temperature [16]. Thus grain boundaries do not affect the electron transport properties at room temperature [26].

Since the BaSnO<sub>3</sub> perovskite structure consists of alternating layers of BaO and SnO<sub>2</sub>, stacking faults including Ruddlesden-Popper-type ones are readily introduced into the microstructure when different crystal domains coalesce during thin film growth [27]. Such structural defects are observed even at the exact Ba/Sn growth stoichiometry and independent from the dislocations resulting from the structural mismatch to the substrate. Therefore, dislocation scattering is investigated as the prevailing mobility-limiting transport mechanism in BaSnO<sub>3</sub> epitaxial films for carrier concentrations below  $1 \times 10^{20} \text{ cm}^{-3}$ . The dislocations which may create trap states for free electrons may explain the significantly reduced doping efficiency when the La impurity concentration is comparable to or smaller than the trap density [28]. The mobility governed by dislocation scattering in a degenerate semiconductor is

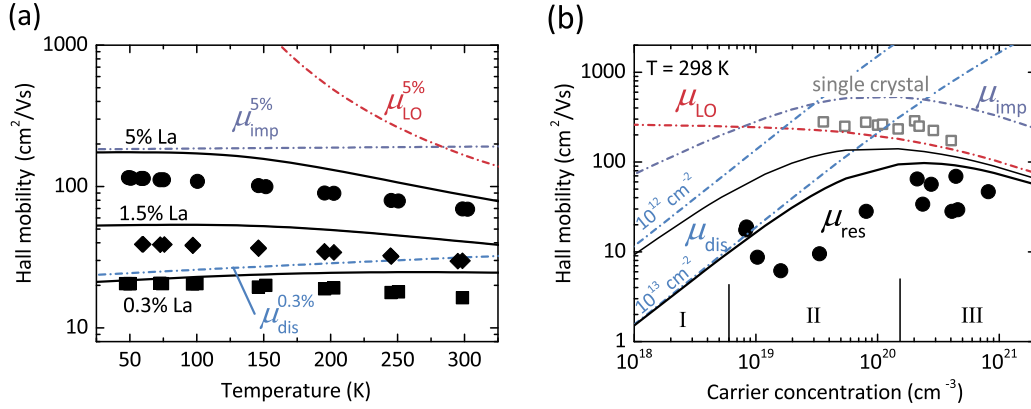


FIG. 4. (a) Temperature-dependent Hall mobility of 0.3%, 1.5%, and 5% La-doped BaSnO<sub>3</sub> films indicates degenerate, metal-like transport behaviors, which are dominated by dislocation scattering for low doping levels and ionized impurity and LO optical phonon scattering for high doping levels. Solid lines present a theoretical calculation of the mobility using the three analytical scattering models according to Eqs. (9), (11), (12), and (15). (b) La:BaSnO<sub>3</sub> films are too resistive to measure Hall voltages for doping levels below 0.3% La (I). The room temperature Hall mobility of the degenerate La:BaSnO<sub>3</sub> films is governed by dislocation scattering in the intermediate-doping regime (II) and LO optical phonon and ionized impurity scattering in the high-doping regime (III). The mobility of La:BaSnO<sub>3</sub> single crystals is given for comparison (gray open squares, after Kim *et al.* [7]).

described by [29]

$$\mu_{\text{dis}} = \frac{8ea^2}{\pi h N_{\text{dis}}} \left( \frac{3n}{\pi} \right)^{2/3} (1 + \xi_0)^{3/2}, \quad (9)$$

where

$$\xi_0 = \frac{\varepsilon_s \varepsilon_0 h^2}{m_c^* e^2} (3\pi^2 n)^{1/3}, \quad (10)$$

and  $a$  is the BaSnO<sub>3</sub> lattice parameter,  $h$  is the Planck constant, and  $N_{\text{dis}}$  is the dislocation density. For carrier concentrations above  $1 \times 10^{20}$  cm<sup>-3</sup>, the room temperature mobility in BaSnO<sub>3</sub> is governed by electron-phonon interactions and electron scattering at ionized La impurities [30]. The mobility governed by LO phonon scattering is calculated according to [31,32]

$$\mu_{\text{LO}\mu} = \frac{1}{2c_\mu \omega_{1\mu}} \frac{e}{m_c^*} \left( 1 + \frac{c_\mu}{6} \right)^{-3} f(c_\mu) \left[ \exp \left( \frac{\hbar \omega_{1\mu}}{k_B T} \right) - 1 \right], \quad (11)$$

where  $c_\mu$  is the electron-phonon coupling constant proportional to the square root of electron effective mass  $\sqrt{m_c^*}$ ,  $\omega_{1\mu}$  is the frequency of the LO phonon mode, and  $f(c_\mu)$  is a slowly varying function ranging from 1.0 to 1.2 for  $0 < c_\mu < 3$  [32]. In La:BaSnO<sub>3</sub>, the three LO phonon modes with  $\hbar \omega_1 = 18, 54,$  and  $91$  meV energy are taken into account [23,24] to calculate an effective mobility  $\mu_{\text{LO}}$  using the sum of reciprocals for each phonon mode, using  $\mu_{\text{LO}}^{-1} = \sum_\mu \mu_{\text{LO}\mu}^{-1}$  [33]. The mobility governed by ionized impurity scattering in a degenerate semiconductor [34,35], taking the nonparabolicity of the conduction band into account [36], is given by

$$\mu_{\text{imp}} = \frac{3\varepsilon_s^2 \varepsilon_0^2 h^3}{m_c^* e^3} \frac{n}{N_i F}, \quad (12)$$

where  $F$  is the screening function

$$F = \left[ 1 + 4 \frac{\xi_1}{\xi_0} \left( 1 - \frac{\xi_1}{8} \right) \right] \ln(1 + \xi_0) - \frac{\xi_0}{1 + \xi_0} - 2\xi_1 \left( 1 - \frac{5}{16} \xi_1 \right) \quad (13)$$

and

$$\xi_1 = 1 - \frac{m_{e0}^*}{m_c^*}. \quad (14)$$

$N_i$  is the concentration of ionized impurities, which is equal to the La concentration assuming that all the La impurity atoms donate one electron each. According to the Matthiessen's rule, the resulting mobility is

$$\mu_{\text{res}}^{-1} = \mu_{\text{dis}}^{-1} + \mu_{\text{LO}}^{-1} + \mu_{\text{imp}}^{-1}, \quad (15)$$

which describes the dependence on temperature and carrier concentration over the entire range of investigation (Fig. 4).

The analysis according to Eqs. (9)–(12) shows that the high La:BaSnO<sub>3</sub> mobility is mainly attributed to two quantities: the small electron effective mass and the large static dielectric constant. The room temperature effective mass increases pronouncedly from  $m_c^* = 0.19$  to  $0.36m_0$  for the range of the carrier concentrations investigated in this work. This is reflected by the large nonparabolicity parameter  $\beta = 0.37$  (eV)<sup>-1</sup> and noticeably reduces the mobility at the highest doping levels concurrent with an increase in the polaron mass. However, the large dielectric constant  $\varepsilon_s = 21$  [23,24] of BaSnO<sub>3</sub> promotes screening of the Coulomb potential of charged dislocations and ionized La impurities [7]. The square dependence of mobility governed by impurity scattering on dielectric constant shows that in contrast to other high-mobility wide-band gap semiconductors such as ZnO ( $\varepsilon_s^\perp = 7.4$  [37]), In<sub>2</sub>O<sub>3</sub> ( $\varepsilon_s = 8.9$  [38]), and GaN ( $\varepsilon_s^\perp = 9.5$  [39]), BaSnO<sub>3</sub> may exhibit a large mobility even at unusually high carrier concentrations because impurity scattering does not become

significant. Furthermore, electron-phonon scattering is less pronounced as compared to other polar oxides such as SrTiO<sub>3</sub> ( $\sim 10 \text{ cm}^2/\text{V s}$  [40]) and Ga<sub>2</sub>O<sub>3</sub> ( $\sim 115 \text{ cm}^2/\text{V s}$  [41]), allowing for an extraordinary high  $\sim 300 \text{ cm}^2/\text{V s}$  mobility even at room temperature [24,30].

Further progress in the development of BaSnO<sub>3</sub> epitaxial films for application in transparent oxide electronics may be realized not only by considering the lattice mismatch with the substrate, but also by optimizing epitaxial growth techniques to reduce dislocation densities and domain boundaries which are inherent to the perovskite structure. Selective area growth and epitaxial lateral overgrowth techniques as successfully applied in III-nitride semiconductor technology [42] may present effective methods for achieving higher mobilities by reducing the dislocation density of the present BaSnO<sub>3</sub> epitaxial films.

In conclusion, the degenerate perovskite BaSnO<sub>3</sub> exhibits an extraordinary high room temperature mobility attributed to an electron effective mass as small as  $0.19m_0$ . An in-depth investigation of the IR free carrier absorption and the Burstein-Moss shift yields a significant dependence of electron effective mass on doping level, concurrent with a pronounced nonparabolicity of the conduction band. The

current room temperature mobility limits in epitaxial films are determined by scattering at dislocations at low doping levels, and ionized impurity scattering and electron-phonon interactions at high doping levels. The large dielectric constant of BaSnO<sub>3</sub> facilitates the screening of charged defects and ionized impurities more than in other transparent semiconductors and electron-phonon scattering is less pronounced as compared to other polar oxide semiconductors, resulting in an enhanced room temperature mobility even at unusually high carrier concentrations.

We thank Dr. J. Jia and Professor Y. Shigesato at Aoyama Gakuin University for assistance with spectroscopic ellipsometry measurements. C.A.N. and M.A.M. acknowledge support from the Leverhulme Trust via M.A.M.'s Research Leadership Award (RL-0072012). M.A.M. acknowledges further support from the Royal Society through a University Research Fellowship. The work at Tokyo Institute of Technology was supported by the MEXT Element Strategy Initiative to Form Core Research Center. H.Hi. was supported by the JSPS through a Grant-in-Aid for Scientific Research on Innovative Areas (Grant No. 25106007), and Support for Tokyotech Advanced Research (STAR).

- 
- [1] H. J. Kim, U. Kim, H. M. Kim, T. H. Kim, H. S. Mun, B.-G. Jeon, K. T. Hong, W.-J. Lee, C. Ju, K. H. Kim, and K. Char, *Appl. Phys. Express* **5**, 061102 (2012).
- [2] C. Park, U. Kim, C. J. Ju, J. S. Park, Y. M. Kim, and K. Char, *Appl. Phys. Lett.* **105**, 203503 (2014).
- [3] U. Kim, C. Park, T. Ha, Y. M. Kim, N. Kim, C. Ju, J. Park, J. Yu, J. H. Kim, and K. Char, *APL Mater.* **3**, 036101 (2015).
- [4] Y. M. Kim, C. Park, U. Kim, C. Ju, and K. Char, *Appl. Phys. Express* **9**, 011201 (2016).
- [5] S. Ismail-Beigi, F. J. Walker, S.-W. Cheong, K. M. Rabe, and C. H. Ahn, *APL Mater.* **3**, 062510 (2015).
- [6] K. Krishnaswamy, L. Bjaalie, B. Himmetoglu, A. Janotti, L. Gordon, and C. G. Van de Walle, *Appl. Phys. Lett.* **108**, 083501 (2016).
- [7] H. J. Kim, U. Kim, T. H. Kim, J. Kim, H. M. Kim, B.-G. Jeon, W.-J. Lee, H. S. Mun, K. T. Hong, J. Yu, K. Char, and K. H. Kim, *Phys. Rev. B* **86**, 165205 (2012).
- [8] H. Mun, U. Kim, H. Min Kim, C. Park, T. Hoon Kim, H. Joon Kim, K. Hoon Kim, and K. Char, *Appl. Phys. Lett.* **102**, 252105 (2013).
- [9] S. Sallis, D. O. Scanlon, S. C. Chae, N. F. Quackenbush, D. A. Fischer, J. C. Woicik, J.-H. Guo, S. W. Cheong, and L. F. J. Piper, *Appl. Phys. Lett.* **103**, 042105 (2013).
- [10] P. V. Wadekar, J. Alaria, M. O'Sullivan, N. L. O. Flack, T. D. Manning, L. J. Phillips, K. Durose, O. Lozano, S. Lucas, J. B. Claridge, and M. J. Rosseinsky, *Appl. Phys. Lett.* **105**, 052104 (2014).
- [11] U. Kim, C. Park, T. Ha, R. Kim, H. S. Mun, H. M. Kim, H. J. Kim, T. H. Kim, N. Kim, J. Yu, K. H. Kim, J. H. Kim, and K. Char, *APL Mater.* **2**, 056107 (2014).
- [12] S. Raghavan, T. Schumann, H. Kim, J. Y. Zhang, T. A. Cain, and S. Stemmer, *APL Mater.* **4**, 016106 (2016).
- [13] W.-J. Lee, H. J. Kim, E. Sohn, T. H. Kim, J.-Y. Park, W. Park, H. Jeong, T. Lee, J. H. Kim, K.-Y. Choi, and K. H. Kim, *Appl. Phys. Lett.* **108**, 082105 (2016).
- [14] C. A. Niedermeier, S. Rhode, S. Fearn, K. Ide, M. A. Moram, H. Hiramatsu, H. Hosono, and T. Kamiya, *Appl. Phys. Lett.* **108**, 172101 (2016).
- [15] H. Mizoguchi, H. W. Eng, and P. M. Woodward, *Inorg. Chem.* **43**, 1667 (2004).
- [16] See Supplemental Material at <http://link.aps.org/supplemental/10.1103/PhysRevB.95.161202> for PLD growth conditions, out-of-plane HR-XRD analysis, IR optical analysis using transmittance/reflectivity and ellipsometry spectra, and experimental details of electron transport measurements.
- [17] S. James Allen, S. Raghavan, T. Schumann, K.-M. Law, and S. Stemmer, *Appl. Phys. Lett.* **108**, 252107 (2016).
- [18] T. Pisarkiewicz, K. Zakrzewska, and E. Leja, *Thin Solid Films* **174**, 217 (1989).
- [19] R. E. Hummel, *Electronic Properties of Materials*, 4th ed. (Springer-Verlag, New York, 2011).
- [20] D. O. Scanlon, *Phys. Rev. B* **87**, 161201 (2013).
- [21] H. Fujiwara and M. Kondo, *Phys. Rev. B* **71**, 075109 (2005).
- [22] K. F. Berggren and B. E. Sernelius, *Phys. Rev. B* **24**, 1971 (1981).
- [23] T. N. Stanislavchuk, A. A. Sirenko, A. P. Litvinchuk, X. Luo, and S.-W. Cheong, *J. Appl. Phys.* **112**, 044108 (2012).
- [24] C. A. Niedermeier, T. Kamiya, and M. A. Moram, *arXiv:1612.01343*.
- [25] Z. Lebens-Higgins, D. O. Scanlon, H. Paik, S. Sallis, Y. Nie, M. Uchida, N. F. Quackenbush, M. J. Wahila, G. E. Sterbinsky, D. A. Arena, J. C. Woicik, D. G. Schlom, and L. F. J. Piper, *Phys. Rev. Lett.* **116**, 027602 (2016).
- [26] J. Y. W. Seto, *J. Appl. Phys.* **46**, 5247 (1975).

- [27] W. Y. Wang, Y. L. Tang, Y. L. Zhu, J. Suriyaprakash, Y. B. Xu, Y. Liu, B. Gao, S.-W. Cheong, and X. L. Ma, *Sci. Rep.* **5**, 16097 (2015).
- [28] N. G. Weimann, L. F. Eastman, D. Doppalapudi, H. M. Ng, and T. D. Moustakas, *J. Appl. Phys.* **83**, 3656 (1998).
- [29] D. Look, C. Stutz, R. Molnar, K. Saarinen, and Z. Liliental-Weber, *Solid State Commun.* **117**, 571 (2001).
- [30] K. Krishnaswamy, B. Himmetoglu, Y. Kang, A. Janotti, and C. G. Van de Walle, [arXiv:1610.06253](https://arxiv.org/abs/1610.06253).
- [31] H. Fröhlich and N. F. Mott, *Proc. R. Soc. London A* **171**, 496 (1939).
- [32] F. E. Low and D. Pines, *Phys. Rev.* **98**, 414 (1955).
- [33] D. M. Eagles, *J. Phys. Chem. Solids* **25**, 1243 (1964).
- [34] H. Brooks, *Adv. Electron. Electron Phys.* **7**, 85 (1955).
- [35] R. Dingle, *Philos. Mag.* **46**, 831 (1955).
- [36] W. Zawadzki and T. S. Moss, in *Handbook of Semiconductors* (North-Holland, Amsterdam, 1982), Chap. 12, p. 713.
- [37] H. Yoshikawa and S. Adachi, *Jpn. J. Appl. Phys.* **36**, 6237 (1997).
- [38] I. Hamberg and C. G. Granqvist, *J. Appl. Phys.* **60**, R123 (1986).
- [39] A. S. Barker and M. Ilegems, *Phys. Rev. B* **7**, 743 (1973).
- [40] A. Verma, A. P. Kajdos, T. A. Cain, S. Stemmer, and D. Jena, *Phys. Rev. Lett.* **112**, 216601 (2014).
- [41] K. Ghosh and U. Singiseti, *Appl. Phys. Lett.* **109**, 072102 (2016).
- [42] K. Hiramatsu, *J. Phys.: Condens. Matter* **13**, 6961 (2001).